Solid-State Electronics 52 (2008) 1606–1609

Contents lists available at ScienceDirect

Solid-State Electronics

journal homepage: www.elsevier.com/locate/sse

A 2D non-parabolic six-moments model

M. Vasicek *, J. Cervenka, M. Wagner, M. Karner, T. Grasser

Institute for Microelectronics, TU Wien, Gußhausstraße 27-29, 1040 Wien, Austria

ARTICLE INFO

Article history:
Received 16 May 2008
Accepted 7 June 2008
Available online 22 July 2008

Review of this manuscript was arranged by A. Iliadis, C. Richter, and A. Zaslavsky

Keywords:
Six-moments model
Subband Monte Carlo
Quantization

ABSTRACT

In order to describe carrier transport in inversion layers we have developed a two-dimensional non-parabolic macroscopic transport model up to the sixth order. To model the transport parameters with as few simplifying assumptions as possible, we apply an extraction technique from Subband Monte Carlo simulations followed by an interpolation within these Monte Carlo tables through the whole inversion layer. Important effects like surface-roughness scattering as well as quantization are inherently considered in the Subband Monte Carlo data, which are used to model higher-order mobilities as well as the macroscopic relaxation times as a function of the effective field and the carrier temperature. The parameters are compared with the results obtained from models using bulk Monte Carlo data, where neither surface roughness nor quantization are considered. The models are applied to a UTB SOI-MOSFET and their predictions are discussed for different gate lengths.

1. Introduction

For gate lengths larger than 25 nm, where source-to-drain tunneling currents can be neglected [1], it is justified to treat carrier transport in lateral direction classically. An accurate way to describe classical transport is to solve the Boltzmann transport equation (BTE), for instance with the time consuming Monte Carlo (MC) technique. However, on an engineering level, an efficient way to find approximate solutions of the BTE is by the method of moments [2]. By multiplying the BTE with special weight functions, making an approximation of the scattering integral with a macroscopic relaxation time and integrating over k-space, one can obtain the drift-diffusion, the energy transport, and the six-moments model [3]. A detailed discussion of this derivation follows in the sequel. The challenge here is to model higher-order transport parameters like the energy relaxation time τ_1, the second-order relaxation time τ_2, the energy mobility μ_1, and the second-order mobility μ_2 (see Fig. 2) as accurately as possible. A good choice is the calculation of parameter tables extracted from MC simulations for a parameter interpolation within a device simulator. So far, bulk MC data has been investigated [4]. There the influence of impurity, acoustic and optical phonon scattering on higher-order transport parameters has been studied. However, the impact of important inversion layer effects like surface-roughness scattering, and the quantization on higher-order parameters have not been taken into account. Hence, using bulk MC data for modeling transport parameters within the inversion layer of a device is insufficient. In [5] surface-roughness scattering has been approximated using the semiempirical Matthiesen rule.

We present a method for modeling these important inversion layer effects as well as a 2D six-moments transport model in order to be consistent with 2D transport in an inversion layer.

2. Transport model

Macroscopic transport models can be systematically derived using the method of moments [6]. Here the moments for the 2D and the 3D case are defined as

$$x_j^D(\mathbf{r}) = \frac{2}{(2\pi)^D}\int_{-\infty}^{\infty} X_j(\mathbf{r},\mathbf{k}) f_D(r,k)\mathrm{d}^D k = n\langle X_j(\mathbf{r},\mathbf{k})\rangle \; = \ll X_j(\mathbf{r},\mathbf{k}) \gg \tag{1}$$

with $x_j(\mathbf{r})$ as the macroscopic values together with the microscopic counterpart $X_j(\mathbf{r},\mathbf{k})$. $f(\mathbf{r},\mathbf{k})$ is the distribution function whereas D is the dimension factor (D = 2 or D = 3) n is the carrier density. Application of these moments to the BTE

$$\partial_t f + \mathbf{v}\cdot\nabla_\mathrm{r} f - q\mathbf{E}\cdot\nabla_\mathrm{p} f = (\partial_t f)_\mathrm{coll}, \tag{2}$$

gives the moment equations for electrons which read

$$\partial_t \ll X_j(\mathbf{r},\mathbf{k}) \gg + \nabla_\mathrm{r} \ll \mathbf{v} X_j(\mathbf{r},\mathbf{k}) \gg + q\mathbf{E} \ll \nabla_\mathrm{p} X_j(\mathbf{r},\mathbf{k}) \gg = \partial_t \ll X_j(\mathbf{r},\mathbf{k}) \gg_\mathrm{coll} \tag{3}$$

$$\partial_t \ll X_j(\mathbf{r},\mathbf{k}) \gg + \nabla_\mathrm{r} \ll \mathbf{v} \otimes X_j(\mathbf{r},\mathbf{k}) \gg + q\mathbf{E} \ll \nabla_\mathrm{p} \otimes X_j(\mathbf{r},\mathbf{k}) \gg = \partial_t \ll X_j(\mathbf{r},\mathbf{k}) \gg_\mathrm{coll} \tag{4}$$

for the even scalar-valued moments and for the odd vector-valued moments, respectively. Eq. (3) is the starting point for the derivation of the balance equations, whereas Eq. (4) describes the fluxes.

* Corresponding author.
E-mail address: vasicek@iue.tuwien.ac.at (M. Vasicek).

0038-1101/$ - see front matter © 2008 Elsevier Ltd. All rights reserved.
doi:10.1016/j.sse.2008.06.010

Here, the even moments X_j are defined as $\langle \epsilon^j \rangle$ and the odd ones are $\langle \mathbf{v}\epsilon^j \rangle$ with $\mathbf{v}$ as the velocity of the carrier, ϵ is the average kinetic energy, and $j \in \mathbb{N}_0$. The odd macroscopic counterparts of these microscopic values are defined here as $n\langle \mathbf{v} \rangle = \mathbf{J_n}$, the current flux, $\langle \mathbf{v}\epsilon \rangle = \mathbf{S}_n$ the energy flux, and $\langle \mathbf{v}\epsilon^2 \rangle = 2/m^* \mathbf{K_n}$ the second-order temperature flux which correspond to the fluxes of the model. The even macroscopic values for 2D are defined [4] as $\ll 1 \gg = n$, $\ll \epsilon \gg = k_B T_n$, and $\ll \epsilon^2 \gg = 2(k_B T_n)^2 \beta$, whereas for 3D the even moments read $\ll 1 \gg = n$, $\ll \epsilon \gg = 3/2 k_B T_n$, and $\ll \epsilon^2 \gg = 15/4(k_B T_n)^2 \beta$. Here β is the kurtosis and denotes the deviation from a heated Maxwellian distribution function and is defined as

$$\beta = \frac{D}{D+2} \frac{\ll \epsilon^2 \gg}{\ll \epsilon \gg^2}. \tag{5}$$

In order to obtain an expression for the right hand side of the BTE that can be handled analytically, a macroscopic relaxation time approximation is introduced. The equations read

$$\partial_t \ll X(r,k) \gg_{\text{coll}}^{\text{even}} \approx -\frac{\ll X(r,k) \gg - \ll X(r,k) \gg_0}{\tau_j} = \frac{x - x_0}{\tau_j}, \tag{6}$$

$$\partial_t \ll X(r,k) \gg_{\text{coll}}^{\text{odd}} \approx -\frac{\ll X(r,k) \gg - \ll X(r,k) \gg_0}{\tau_j} = -\frac{J_j}{\tau_j}, \tag{7}$$

for the balance as well as for the flux equations, respectively. Here, J_j are the fluxes in the transport equations. Within the relaxation time approximation the moments relaxes to its equilibrium state with the time constant τ_j after removing all driving fields. In the diffusion approximation [7], the non-diagonal tensorial components in the fluxes vanish. Putting everything together, the six-moments model reads

$$\phi_0 : D_0 \partial_t n - \frac{1}{q_0} \nabla_r \mathbf{J_n} = 0, \tag{8}$$

$$\phi_2 : D_2 k_B \partial_t (n T_n) + \nabla_r \mathbf{S}_n - \mathbf{E} \cdot \mathbf{J_n} = -D_2 n k_B \frac{T_n - T_0}{\tau_1}, \tag{9}$$

$$\phi_4 : D_4 \frac{k_B^2}{m^*} \partial_t (n T_n^2 \beta) + \frac{2}{m^*} \nabla_r \mathbf{K_n} + \frac{4 q_0}{m^*} \mathbf{E} \cdot \mathbf{S}_n = -D_4 c \frac{T_n^2 \beta - T_0^2}{\tau_2}, \tag{10}$$

$$\phi_1 : \mathbf{J_n} = \mu_0 H_0 (D_1 \nabla_r (k_B n T_n) + h_0 q_0 \mathbf{E} n), \tag{11}$$

$$\phi_3 : \mathbf{S}_n = -\mu_1 H_1 \left(D_3 \nabla_r \left(n \frac{(k_B T_n)^2}{q} \beta \right) + h_1 D_3 k_B T_n \mathbf{E} n \right), \tag{12}$$

$$\phi_5 : \mathbf{K_n} = -\mu_2 H_2 \left(D_5 \nabla_r \left(n \frac{(k_B T_n)^3}{q} \gamma \right) + h_2 D_5 (k_B T_n)^2 \mathbf{E} n \beta \right), \tag{13}$$

with $D_0 = 1$, $D_1 = 1$, $D_2 = D/2$, $D_3 = (2 + D)/2$, $D_4 = (2 + D)D/2^{4-D}$, and $D_5 = (4 + D)(2 + D)/4$ as the dimension factors of the transport model. (D = 2 for two dimensions, and D = 3 for three dimensions), and H_i the non-parabolicity factors [4]. For parabolic bands, H_i equals unity. Each moment equation contains information on the next higher one. As a consequence one has to truncate the equation hierarchy in order to get a fully defined equation set. Most important is the closure relation, which includes the information of the higher-order moments and thus determines the accuracy of the system. For instance, in the case of the drift-diffusion model the electrons are assumed to be in thermal equilibrium ($T_n = T_L$) with the lattice [8] whereas the closure relation of the six-moments model is linked to the kurtosis [9] and empirically described as β^c with $c = 2.7$ [4]. A description of the non-parabolic energy transport model with the closure relations used in the device simulator is given in [4]. Furthermore all macroscopic models are discretized using an extended Scharfetter-Gummel type scheme [4].

Another crucial step is the modeling of the transport parameters. In order to account for quantization effects and surface-roughness scattering, a self-consistent coupling of a Subband Monte Carlo simulator (SMC) and a Schrödinger–Poisson (SP) solver (see Fig. 1) has been developed [10,11]. The SP solver solves the quantum confinement and the SMC simulator calculates 2D transport in each subband [12]. Convergence is reached by an exchange of energies, wavefunctions, and subband occupations (see Fig. 1). Hence, higher-order parameters like the second-order mobility μ_2 (see Fig. 2) can be extracted. This has been done for different effective fields. In order to study the higher-order parameter behavior through a whole device, our device simulator Minimos-NT [13] calculates the effective field through the channel and interpolates mobilities as well as relaxation times corresponding to the effective field using the pre-calculated SMC tables. In the drain and source regions, where no quantization is considered, fullband bulk MC tables are used. In the case of the energy transport and the six-moments model, an additional interpolation parameter within the MC table is the average energy. So higher-order parameters μ_j and τ_j read as $\mu_j(E_{\text{eff}}, T_n)$ and $\tau_j(E_{\text{eff}}, T_n)$, whereas in the drift-diffusion model the additional parameter is the driving field. Hence the mobility μ_0 can be written as $\mu_0(E_{\text{eff}}, E)$.

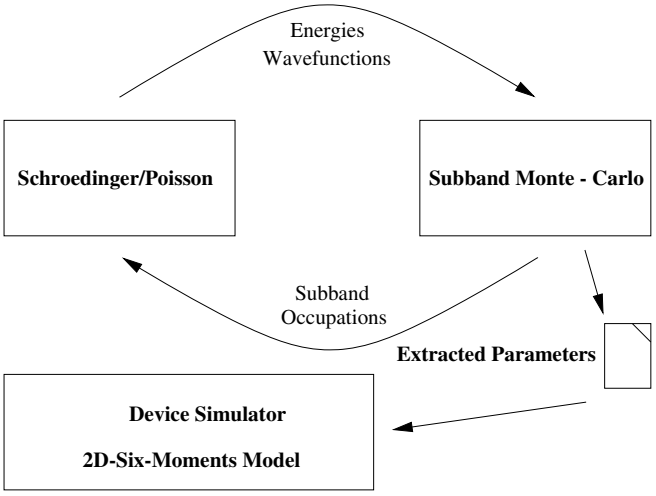

Fig. 1. Transport parameters of a 2D electron gas in an inversion layer are extracted self-consistently and modeled through a whole device with a device simulator.

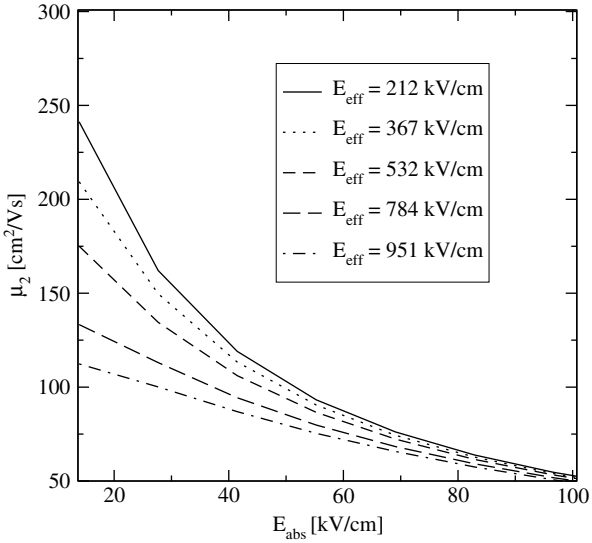

Fig. 2. Extracted second-order mobility as a function of the driving field for different effective fields. The device simulator interpolates between these curves.

3. Results and discussion

The transport models are divided into two parts. The microscopic part corresponding to the SMC extractions and a macroscopic part coming from the method of moments. To determine both parts of the model, UTB SOI-MOSFETs with a bulk thickness of 4 nm and several gate lengths are investigated.

Fig. 3 shows the second-order temperature and the carrier temperature with respect to the lateral coordinate of a 40 nm gate length device. By increasing the drain voltage, the deviation of these two temperatures increases as well. Since the second-order temperature is defined as the kurtosis times the carrier temperature, the difference between these two temperatures is an indication of the deviation of the distribution function from a heated Maxwellian. The kurtosis reaches a maximum at the end of the channel, where hot electrons meet cold electrons from the drain region. This yields a mixture of a hot and cold distribution function. The kurtosis increases as well in transistors with decreasing gate lengths, where strong electric fields generate electrons very far away from equilibrium. Therefore, the drift-diffusion model, which is accurate for devices with channel lengths down to 100 nm, loses its validity [14].

In Fig. 4, higher-order mobilities based on SMC data and bulk MC data are plotted. It clearly shows the importance to use SMC data for modeling transport properties in UTB transistors. Furthermore, surface-roughness scattering is included in the 2D model.

The velocity profiles of the three transport models calculated for a 40 nm and a 60 nm gate length device are presented in Fig. 5.

The spurious velocity overshoot in the energy transport model is reduced in the six-moments model, as can be observed in both devices. As pointed out in [15] this is due to the closure relation and the modeling of the relaxation times and cannot be eliminated completely using a finite number of moment equations. This veloc-

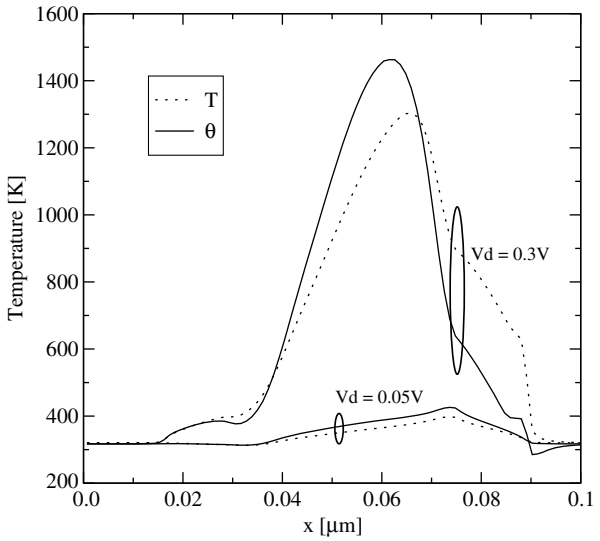

Fig. 3. The second-order temperature $\theta = \beta T$ in comparison to the carrier temperature T. With increasing drain voltage, the deviation from the Maxwellian distribution ($\theta \approx T$, $\beta \approx 1$) increases.

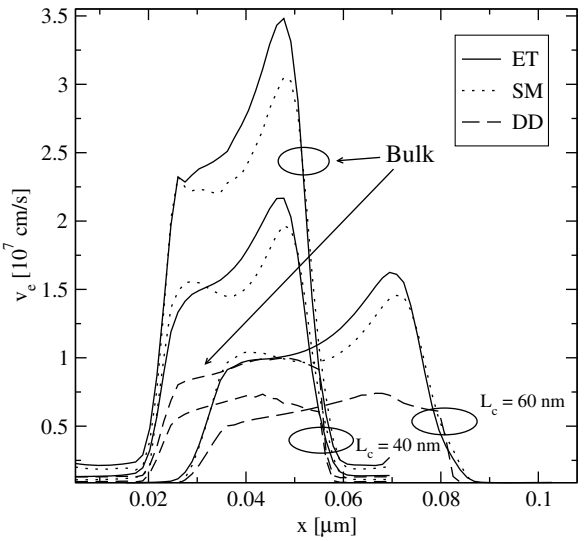

Fig. 5. A velocity profile calculated with the drift-diffusion, energy transport, and the six-moments model for 40 nm and 60 nm SOI-MOSFETs. The 40 nm device is as well calculated with bulk data, where no quantum effects are considered.

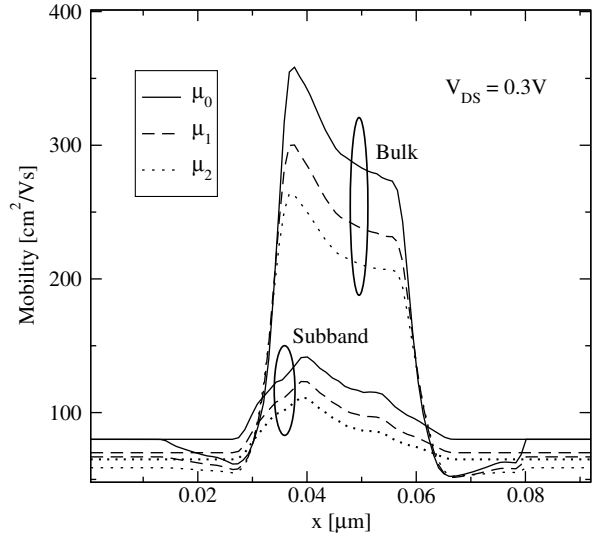

Fig. 4. A comparison between higher-order mobilities calculated with SMC data and bulk MC data through an SOI-MOSFET with a gate length of 40 nm. Due to surface-roughness scattering, the subband mobilities are lower than the bulk mobilities.

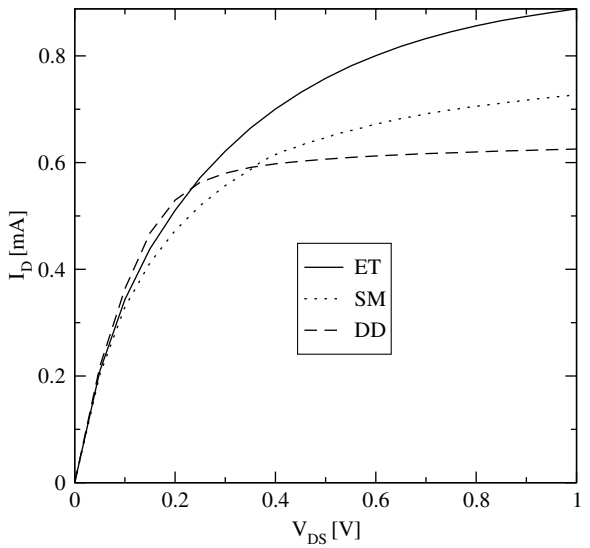

Fig. 6. The Output characteristics calculated with the drift-diffusion, energy transport, and the six-moments model of a UTB SOI-MOSFET.

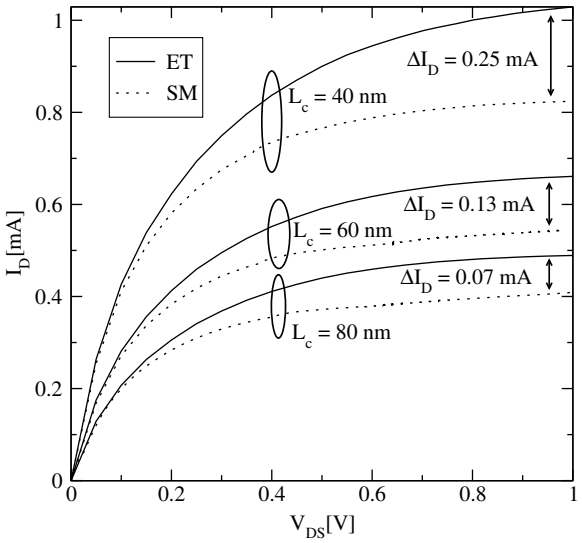

Fig. 7. Output characteristics calculated with the energy transport and the six-moments model for SOI-MOSFETs with 40 nm, 60 nm, and 80 nm gate lengths. With increasing gate length the difference in the currents decrease.

ity overshoot leads to an overestimation of the output characteristics of the energy transport model.

In Fig. 6 we present the output characteristics of a 40 nm channel length SOI device calculated with the drift-diffusion, energy transport and the six-moments model. The output current predicted by the drift-diffusion calculations is smaller compared to the other models. This can be explained with the velocity profiles of Fig. 5.

As a consistency check [16] for long channel devices all models must yield the same results. We show in Fig. 7 output characteristics from the energy transport and the six-moments model for several SOI MOSFETs with different gate lengths. The differences in the current of the two transport models decrease with further increase of the channel length.

4. Summary and conclusion

We have developed a 2D non-parabolic six-moments model based on SMC data in order to accurately model carrier transport in inversion layers of aggressively scaled devices. This approach allows the investigation of UTB SOI devices including the influence of surface-roughness scattering and quantization within higher-order moment models. A generalized set of equations has been used to derive the 3D bulk model and a novel 2D model. A crucial step is the modeling of the transport parameters which has been discussed in detail. The model has been used to investigate UTB SOI-MOSFETs with different channel lengths. First, it has been shown that the transport properties of UTB SOI devices cannot be accurately reproduced using bulk models. Second, the importance of using higher-order moment models for the modeling of devices with a gate length in the deca-nanometer regime has been proven.

Acknowledgement

This work has been supported by the Austrian Science Fund project P18316-N13.

References

[1] Sverdlov V, Grasser T, Kosina H, Selberherr S. Scattering and space-charge effects in Wigner Monte Carlo simulations of single and double barrier devices. J Comput Elect 2006;5:447–50.
[2] Grasser T, Kosina H, Gritsch M, Selberherr S. Using six moments of Boltzmann's transport equation for device simulation. J Appl Phys 2001;90(5):2389–96.
[3] Anile A, Muscato O. Improved hydrodynamical model for carrier transport in semiconductors. Phys Rev B 1995;51(23):16728–40.
[4] Grasser T, Kosik R, Jungemann C, Kosina H, Selberherr S. Nonparabolic macroscopic transport models for device simulation based on Bulk Monte Carlo data. J Appl Phys 2005;97(9):093710-1–093710-12.
[5] Neinhüs B, Nguyen C, Jungemann C, Meinerzhagen B. A CPU efficient electron mobility model for MOSFET simulation with quantum corrected charge densities. In: Proc ESSDERC, (Cork, Ireland). p. 332–5, Frontier Group; September 2000.
[6] Blotekjaer K. Transport equations for electrons in two-valley semiconductors. IEEE Trans Electron Dev 1970;ED-17:38–47.
[7] Thoma R, Emunds A, Meinerzhagen B, Pfeifer H-J, Engl W. Hydrodynamic Equation for Semiconductors with Nonparabolic Band Structure. IEEE Trans Electron Dev 1991;38:1342–53.
[8] Grasser T, Tang T, Kosina H, Selberherr S. A review of hydrodynamic and energy-transport models for semiconductor device simulation. Proc IEEE 2003;91:251–74.
[9] Grasser T. Non-parabolic macroscopic transport models for semiconductor device simulation. Physica A 2005;349(1/2):221–58.
[10] Vasicek M, Karner M, Ungersboeck E, Wagner M, Kosina H, Grasser T. Modeling of macroscopic transport parameters in inversion layers. In: International conference on simulation of semiconductor processes and devices 2007; 2007.
[11] Vasicek M, Cervenka J, Karner M, Wagner M, Grasser T.Parameter modeling for higher-order transport models in UTB SOI MOSFETs. In: 12th international workshop on computational electronics book of abstracts; 2007. p. 96–7.
[12] Lucci H, Esseni D, Palestri P, Selmi L. Comparative analysis of basic transport properties in the inversion layer of bulk ans SOI MOSFETs: a Monte-Carlo study. In: Proc ESSDERC; 2004. p. 321–4.
[13] http://www.iue.tuwien.ac.at/software/minimos-nt, "Minimos-NT 2.0 User's Guide, IμE." Institut für Mikroelektronik, Technische Universität Wien, Austria; 2002.
[14] Jungemann C, Grasser T, Neinhüs B, Meinerzhagen B. Failure of moments-based transport models in nanoscale devices near equilibrium 2005; 52(11):2404–8.
[15] Grasser T, Kosina H, Selberherr S. Investigation of spurious velocity overshoot using Monte Carlo data. J Appl Phys Lett 2001;79(12):1900–2.
[16] Grasser T, Jungemann C, Kosina H, Meinerzhagen B, Selberherr S. Advanced Transport models for sub-micrometer devices. In: Proc SISPAD, p. 1–8; 2004.